2019

Performance analysis of a thermal-driven tubular direct contact membrane distillation system

Abdellah Sharifian
Edith Cowan University

Mehdi Khiadani
Edith Cowan University

Ataollah Nosrati
Edith Cowan University

10.1016/j.applthermaleng.2019.113887
Shafieian, A., Khiadani, M., & Nosrati, A. (2019). Performance analysis of a thermal-driven tubular direct contact membrane distillation system. *Applied Thermal Engineering*, *159*, Article 113887. Available here

This paper has been published as: Shafieian, A., Khiadani, M., & Nosrati, A. (2019). Performance analysis of a thermal-driven tubular direct contact membrane distillation system. *Applied Thermal Engineering, 159*, Article 113887. doi:10.1016/j.applthermaleng.2019.113887

Performance analysis of a thermal-driven tubular direct contact membrane distillation system

Abdellah Shafieian, PhD Candidate, School of Engineering, Edith Cowan University, 270 Joondalup Drive, Joondalup, Perth, WA 6027, Australia

Email: a.shafieiandastjerdi@ecu.edu.au

Mehdi Khiadani, Associate Professor, School of Engineering, Edith Cowan University, 270 Joondalup Drive, Joondalup, Perth, WA 6027, Australia. Tel.: +61 8 6304 5825; fax: +61 8 6304 5811.

Email: m.khiadani@ecu.edu.au (author for correspondence)

Ataollah Nosrati, Lecturer, School of Engineering, Edith Cowan University, 270 Joondalup Drive, Joondalup, Perth, WA 6027, Australia

Email: a.nosrati@ecu.edu.au

Abstract

This paper examines the performance of a thermal-driven tubular direct contact membrane distillation (DCMD) system theoretically and experimentally. A multi-step mathematical model was developed to predict the fresh water productivity of the tubular DCMD module applicable for both small and large-scale applications by considering the changes in the operational variables along the membrane's length. The proposed model was verified by building an experimental rig which was tested under different operational conditions. The results showed that keeping the mass flow rates in the hot and cold channels either near the end or beyond the transition range of the flows results in higher water production. In addition, heating up the feed stream is more efficient for enhancing the water productivity than using the same amount of energy to cool the permeate stream down. Finally, the effects of operational and physical factors on the fresh water productivity of were identified and discussed.

Keywords: Desalination; Membrane; Fresh water productivity; Heat and mass transfer

Nomenclature

A	Area (m^2)	P	Pressure (Pa)
a	Air	p	Permeate
cv	Control volume	Q	Heat flux (W/m^2)
C_m	Membrane specific mass transfer coefficient (kg/m^2sPa)	R	Gas constant (J/kg.K)
D	Diffusion coefficient	Re	Reynolds number
D_h	Hydraulic diameter (m)	r	Pore radius (m)
D_m	Molecular diffusivity (m^2/s)	S	Salinity
D_{w-a}	Water vapour diffusion coefficient	Sh	Sherwood number
d	Pore dimension (m)	T	Temperature (°C)
d_e	Vapour and air collision diameter (m)	t	Time
E	Energy rate (W)	U	Overall heat transfer coefficient (W/m^2K)
f	Feed	V	Velocity (m/s)
H_v	Evaporation enthalpy (J/kg)	v	Vapour
h	Convective heat transfer coefficient (W/m^2K)	W	Transferred molecules mean free path (m)
J	Transmembrane water flux (kg/m^2s)	w	Water
K	Film mass transfer coefficient (m/s)	Y	Specific enthalpy (J/kg)
K_b	Boltzmann constant		
K_g	Water vapour thermal conductivity inside the pores (W/m.K)	**Greek letters**	
k_m	Membrane module thermal conductivity (W/m.K)	δ	Thickness (m)
L	Length (m)	ρ	Density (kg/m^3)
M	Molecular weight (kg/mol)	ε	Porosity
m	Membrane surface/mass flow rate (kg/s)	μ	Dynamic viscosity (m^2/s)
n	Step/section number	τ	Membrane tortuosity

1. Introduction

Water shortage has affected millions of people around the world and predictions evaluate the situation in the future as warning. Many researchers have tried to combat this global issue and various methods of desalination such as reverse osmosis and solar stills have been proposed. However, different practical and economic complications, including low water quality and low productivity of solar stills and polarization films formation, fouling generation, and high energy demand of reverse osmosis systems, have restricted their application [1-4]. To overcome abovementioned problems, a new technology called Membrane Distillation (MD) has been proposed which takes advantage of an advanced separation technique to produce potable water from saline water [5].

Membrane-based desalination technique has several noticeable advantages such as low heat loss, less pre-treatment requirements, low operating pressures, and higher efficiently [6]. In addition, moderate temperatures can create the driving force for the membrane which enables the coupling of membrane-based systems with solar, geothermal energy, and waste heat resources to minimize the water production cost [5]. Moreover, the operation of a MD unit is often simple and requires the least equipment [7].

Membrane module includes two channels for hot (feed) and cold (permeate) flow streams which are separated by a membrane module having a specific porosity [8]. Water molecules evaporate from saline water and transfer from the feed stream having higher vapour pressure to the permeate stream having lower vapour pressure. The main driving force for mass transfer across the membrane module is the vapour pressure difference which is created as a result of the temperature difference [9]. The existence of these thermal processes (i.e. evaporation and condensation) is the main reason for the existence of the temperature and concentration gradient in the liquid films near the membrane surfaces which leads to creation of boundary layers. As a result, the membrane surfaces/sides temperatures as well as concentrations are

different from the flow streams mean values of these parameters inside the cold and hot channels.

To obtain the produced fresh water, the vapour pressure difference between walls of the membrane should be multiplied by the specific mass transfer coefficient (MTC) of the membrane. The MTC is calculated using three mechanisms called Poiseuille flow, Knudsen diffusion, and Molecular diffusion [9]. Also, a combination of these mechanisms can be used by considering them as mass transfer resistances and arranging them in parallel and series configurations. To date, many researchers have investigated the performance of DCMD systems experimentally and theoretically using the abovementioned mass transfer mechanisms [10-13]. Gabelmana and Hwang [14] comprehensively reviewed the operating principles, applications, and relevant mathematics of hollow fibre membrane contactors.

Karam et al. [15] applied energy and mass conservation equations and proposed a dynamic model with satisfactory accuracy for performance investigation of flat-sheet direct contact membrane-based systems. Chen et al. [16] used a 2-D theoretical model to study the pure water productivity of flat-sheet membrane-based systems. The combined Poiseuille-Knudsen flow model showed a good accuracy for laminar flows when it was compared with the experimental results. Guo et al. [17] integrated flat-sheet membrane distillation modules with evaporative crystallizer and simulated the performance of the zero liquid discharge water desalination system. The results were used to determine the optimum values of operational and dimensional parameters of the system.

Lawal and Khalifa [18] proposed the application of a novel regression model to predict the performance of a flat-sheet DCMD unit. They also applied statistical analysis of variance to investigate the effect of each operational parameter on water productivity of the membrane. In another study, Ho et al. [19] applied the separated variable method to analyse the effect of

various operation conditions on the efficiency of a tubular hollow-fibre DCMD unit. The orthogonal expansion technique was used to solve the conjugated Graetz problem. In a theoretical and experimental study, Bardesco et al. [20] studied the adiabatic absorption process of membrane distillation modules under different operational conditions. The developed model resulted in an evolutionary study of the major parameters in both axial and radial directions of the membrane module.

Eleiwi et al. [21] used a theoretical dynamic model for analysing the performance of flat-sheet DCMD modules which are powered by intermittent energy supplies. Two dimensional advection–diffusion equations were considered as a base to analyse the heat and mass transfer processes. In a similar study, Bhattacharya et al. [22] developed a 2-D mathematical model to study the chromium (VI) removal performance of a flat-sheet DCMD system. The coupled Poiseuille and Knudsen models were applied to simulate the mass transfer through the membrane module. Zhou et al. [23] used heat and mass balance equations to simulate the performance of flat-sheet membrane distillation modules in a liquid desiccant air conditioning system. The accurate developed model provided the ability of analysing the performance of the system under different operational parameters and climatic conditions.

Nakoa et al. [6] connected the flat-sheet DCMD module to a salinity gradient solar pond and evaluated the performance of the coupled system both experimentally and theoretically. Doung et al. [24] proposed a brine recycling technique to enhance the thermal efficiency of a flat-sheet membrane-based unit. In the proposed system, the sensible energy of the returning brine was recovered inside the feed tank in the form of heat.

Elzahaby et al. [7] evaluated the effect of geometric and operational conditions on the performance of a solar tubular membrane-based desalination system both experimentally and theoretically. In a similar study, Kabeel et al. [25] used solar energy to drive a tubular DCMD

system and the results indicated the maximum productivity of 33.55 L/day. Shim et al. [26] developed a mathematical model to investigate the water productivity of the flat-sheet membrane module in a solar assisted DCMD system in unsteady state conditions.

Park et al. [27] studied the effect of using screen spacers on temperature and concentration polarization of flat-sheet DCMD modules both theoretically and experimentally. Elmarghany et al. [28] investigated the thermal performance of flat-sheet DCMD modules experimentally. Similar theoretical and experimental studies on the performance of different types of DCMD modules can be found in the literature [29-34].

Most of the previous studies have not considered the changing nature of the operational parameters (e.g., salinity, temperature, and mass flow rate) along the membrane's length. Ignoring the changing trend of these parameters along the membrane's length may lead to little errors at the bench-scale research experiments, however, it is likely to result in noticeable errors in long membranes and large-scale applications. On the other hand, another group of proposed models are too complex imposing excessive economic costs and increase computational processing times [21]. In addition, most of the previous investigations have mainly focused on flat-sheet membrane modules, have not taken the experimental and theoretical observations beyond common trends, and also have not considered the effects of concentration and temperature polarizations.

Therefore, the objective of this study is to provide a comprehensive theoretical and experimental investigation on the performance and fresh water productivity of a tubular DCMD system. A multi-step iterative theoretical model was developed to investigate the performance of the membrane module and was generalized in a way to reduce the computation costs and at the same time to maintain the accuracy especially for large-scale applications. Moreover, an experimental rig was built, tested under different operational conditions, and used to compare

the theoretical results obtained from the developed model with the experimental data. Finally, the effects of various parameters on temperature polarization and gain output ratio of the tubular membrane was studied in details.

2. Mathematical modelling

Figure 1 depicts the structure of the tubular DCMD module which consists of several feed channels covered in a shell that has 4 inlet and outlet ports. For determination of the temperature and salinity distribution along the membrane module, it should be discretised into smaller sections which are perpendicular to the stream direction (Fig. 1). The equations of heat and mass processes along with the energy and mass balance equations should be solved for each of these sections named as steps. The outlet parameters of each section provide the inlet boundary conditions for the next section. Discretization proceeds from the feed stream inlet to its outlet for both feed and permeate channels. Therefore, the subscript n, which shows the inlet conditions of the feed stream sections, represents the outlet conditions of the permeate stream sections (Fig. 1). It is worth noting that due to small diameter of the DCMD module and its large length to diameter ratio, the permeate flow is assumed to be unidirectional.

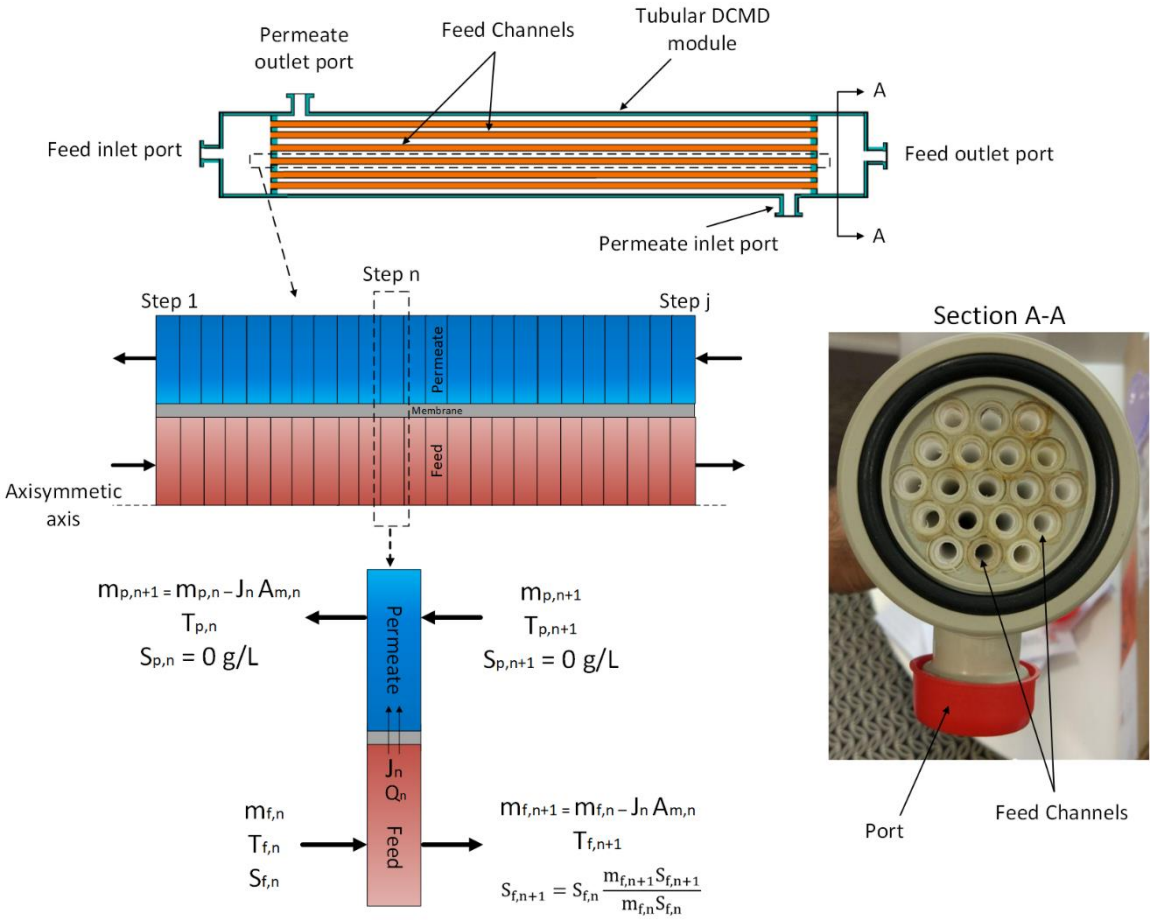

Fig. 1. The membrane which is discretised into smaller sections along with inlet and outlet boundary conditions of each section.

2.1. Energy and mass balance

By assuming that the potential energy across each section is constant and there is no energy input in form of work, the steady state energy balance equations for both feed and permeate streams consist of two main components which are transferred energies by heat and mass [35]:

$$E_{f-n,in} - E_{f-n,out} = \frac{dE_{f-cv}}{dt} \tag{1}$$

$$E_{f-n,in} = E_{f-n,out} \tag{2}$$

$$m_{f,n}\left(Y_{f,n} + \frac{V^2{}_{f,n}}{2}\right) = m_{f,n+1}\left(Y_{f,n+1} + \frac{V^2{}_{f,n+1}}{2}\right) + Q_n A_{m,n} \tag{3}$$

$$m_{p,n}\left(Y_{p,n} + \frac{V^2{}_{p,n}}{2}\right) = m_{p,n+1}\left(Y_{p,n+1} + \frac{V^2{}_{p,n+1}}{2}\right) + Q_n A_{m,n} \tag{4}$$

The mass flow rate of each section is different from the previous section and can be calculated for feed and permeate streams by:

$$m_{f,n+1} = m_{f,n} - J_{w,n}A_{m,n} \quad (5)$$

$$m_{p,n+1} = m_{p,n} - J_{w,n}A_{m,n} \quad (6)$$

2.2. Heat and mass transfer

The following assumptions are considered for modelling heat and mass transfer in the tubular DCMD module [35]: (i) both the feed flow in the hot channel and the permeate flow in the cold channel remain in the steady state and the incompressible situation; (ii) heat loss to the surroundings is negligible; (iii) the mass transfer due to the motion of fluid mixtures through porous media is considered to obey the Dusty-Gas model; and (iv) cold permeate water's momentum through the membrane is neglected.

The mass transfer in a DCMD module has been proved to be in linear relationship with the vapour pressure difference defined as [36]:

$$J_w = C_m\left[P_v(T_{f,m}, S_{f,m}) - P_v(T_{p,m}, S_{p,m})\right] \quad (7)$$

Thermo-physical characteristics of water were calculated using the equations presented by Sharqawy et al. [37]. The heat and mass transfer coefficients along with the temperature and salinity at the membrane surfaces should be calculated as follows to determine the mass flux through the membrane.

2.2.1. Heat transfer

The heat transfer theoretical model of the membrane desalination system is divided into three sections (Fig. 2): (i) thermal energy that is transmitted from the hot water inside the feed channel to the boundary layer which forms adjacent to the membrane wall (Q_f); (ii) combined heat that is transmitted by both the conduction through membrane and the water vapour

movement through the pores (Q_m); and (iii) thermal energy is transmitted from the permeate boundary layer to the permeate cold water (Q_p) [38].

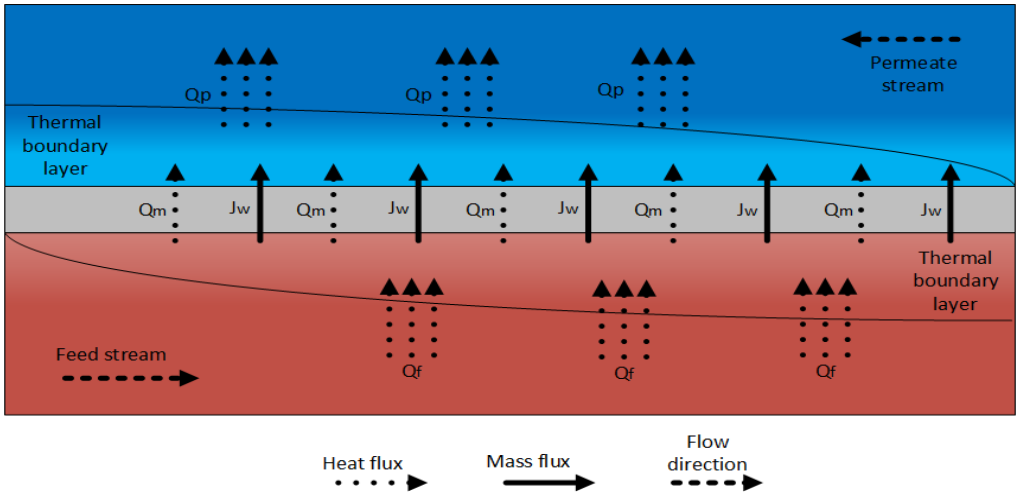

Fig. 2. Schematic diagram of heat transfer process in DCMD modules

Q_f, Q_m, and Q_p are defined as:

$$Q_f = h_f\left(T_f - T_{f,m}\right) \tag{8}$$

$$Q_m = h_m\left(T_{f,m} - T_{p,m}\right) + J_w H_v(T_{f,m}, S_{f,m}) \tag{9}$$

$$Q_p = h_p\left(T_p - T_{p,m}\right) \tag{10}$$

In Eq. (9), h_m (W/m^{2}K) can be obtained from:

$$h_m = \frac{k_g\varepsilon + k_m(1-\varepsilon)}{\delta} \tag{11}$$

According to steady state assumption:

$$Q_m = Q_f = Q_p = Q \tag{12}$$

Total heat rate that is moved through the membrane can be obtained from:

$$Q = U\left(T_f - T_p\right) = \left[\frac{1}{h_f} + \frac{1}{h_m + \frac{J_w H_v}{\left(T_{f,m} - T_{p,m}\right)}} + \frac{1}{h_p}\right]^{-1}\left(T_f - T_p\right) \tag{13}$$

The boundary layers' convective heat transfer coefficients in hot and cold channels are functions of geometrical, operational, and thermo-physical parameters. Equations for calculating Nusselt and Sherwood numbers, which are provided in the literature [39-45], can be used to obtain the convective heat and mass transfer coefficients.

2.2.2. Mass transfer

The salinity at the membrane surface was determined by using the mass balance equation and film theory on the feed side boundary layer [46]:

$$S_{f,m} = S_f \exp\left(\frac{J_w}{\rho_f K}\right) \tag{14}$$

The film mass transfer coefficient (K) can be obtained by using Sherwood number (Sh) which can be obtained by [47]:

$$Sh = \frac{K D_h}{D_m} \tag{14}$$

$$Sh = 0.13 Re^{0.64} Sc^{0.38},\ Re < 2100 \tag{15}$$

$$Sh = 0.23 Re^{0.8} Sc^{0.33},\ Re > 2100 \tag{16}$$

The dimensionless parameter of *Sc* in the abovementioned equations Schmidt number which can be calculated by [47]:

$$Sc = \frac{\mu}{\rho D_m} \tag{17}$$

The readers are referred to [38, 48, 49] for further information regarding detailed process of convective mass transfer calculations.

Knudsen number has been introduced to specify a quantitative measurement for determining flow type [50].

$$Kn = \frac{W}{d} \tag{18}$$

Three different types of flow mechanism can take place inside the membrane considering the different ranges of Knudsen number (*Kn*) [38]. For *Kn*<0.01, the flow is specified as molecular diffusion, in which molecule-molecule collisions are predominant instead of molecule-pore surface collisions. For *Kn*>1, the flow is specified as Knudsen mechanism that is completely opposite to the molecular diffusion, and *Kn* between 0.01 and 1 is specified as transition process that is called Knudsen-molecular diffusion. However, it should be noted that in some references, the transition range is extended up to 10 and *Kn* between 0.01 and 10 is considered as transition region [51].

The average transported molecules free path is calculated by [6]:

$$S = \frac{K_b T}{1.44\pi P d_e^2} \tag{19}$$

C_m for Knudsen flow mechanisms is obtained by [9]:

$$C_m = \frac{2}{3}\frac{\varepsilon r}{\tau\delta}\left(\frac{8M}{\pi RT}\right)^{0.5} \tag{20}$$

C_m for molecular diffusion is obtained from [8]:

$$C_m = \frac{\varepsilon r}{\tau\delta}\frac{PD}{P_a}\frac{M}{RT} \tag{21}$$

C_m for Knudsen-molecular diffusion transition mechanism is calculated by Eq. (22) [8]:

$$C_m = \left[\frac{2}{3}\frac{\varepsilon r}{\tau\delta}\left(\frac{8M}{\pi RT}\right)^{0.5} + \frac{\varepsilon r}{\tau\delta}\frac{PD}{P_a}\frac{M}{RT}\right] \tag{22}$$

The correlations presented by [52] was used to calculate the tortuosity of the DCMD module and its value was obtained to be 1.5.

An iterative computer modelling should be implemented to calculate $T_{f,m}$ and $T_{p,m}$. The program starts by estimating the temperature of the hot and cold membrane surfaces. These values are presumed to be equivalent to T_f and T_p that are the bulk temperatures of feed and product

streams, respectively. The heat transfer coefficients is estimated by (i) entering input geometrical parameters and (ii) calculating operational and thermo-physical parameters. Then, the calculated heat transfer coefficients are used to define new quantities of $T_{f,m}$ and $T_{p,m}$ using Eq. (23) and (24).

$$T_{f,m} = \frac{h_m\left(T_p + \left(\frac{h_p}{h_f}\right)T_f\right) + h_f T_f + J_w H_v}{h_m + h_f\left(1 + \frac{h_m}{h_p}\right)} \tag{23}$$

$$T_{p,m} = \frac{h_m\left(T_f + \left(\frac{h_p}{h_f}\right)T_p\right) + h_p T_p + J_w H_v}{h_m + h_p\left(1 + \frac{h_m}{h_f}\right)} \tag{24}$$

Repeating this process by a number of iterations will allow to specify the final values of $T_{f,m}$ and $T_{p,m}$ with acceptable precision and move to the last step to calculate other parameters such as the fresh water production rate.

2.3. Multi-step process

Figure 3 indicates the flowchart of the computation process developed in this study for theoretical modelling the DCMD module. With the aim of determining the temperature and salinity distribution along the membrane module, heat and mass transfer equations for a single section (Eq. (7)-(24)) should be applied. Then, mass and energy balance equations (Eq. (1)-(6)) should be used to calculate the inlet conditions of the next section. Combination of Eq. (3) and (4) results in an equation with the outlet temperature and salinity as the unknown parameters. The salt mass balance equation (Eq. (25)) provides an additional equation to eliminate one of the unknowns. As the produced equation is not linearly related to the outlet temperature, numerical methods such as Secant Method should be used to solve it.

$$\frac{m_{f,n}}{\rho_{f,n}} S_{f,n} = \frac{m_{f,n+1}}{\rho_{f,n+1}} S_{f,n+1} \tag{25}$$

The mathematical model starts with initial guesses of total water flux through the membrane (J_{wa}) and outlet temperature of the permeate stream (T_a). Using the abovementioned procedure and by applying the below boundary conditions (Eq. (26)-(35)), the inlet temperature of the permeate stream should be calculated and compared with the actual value. If the difference is not within the specified error range, the initial guess should be changed. The calculations should be repeated until an acceptable difference (0.0001 °C) between the calculated and actual outlet temperature is reached. The same process should be repeated for the inlet mass flow rate of the permeate stream. It's worth mentioning that finding the optimum number of steps plays an important role in computation time and 20 was obtained to be the optimum step number in all the theoretical simulations of this study.

$$m_w = \sum_{n=1}^{n=j} J_{w,n} A_{m,n} \tag{26}$$

$$T_{f,0} = T_{f,in} \tag{27}$$

$$T_{f,j} = T_{f,out} \tag{28}$$

$$T_{d,0} = T_{f,in} - T_a \tag{29}$$

$$T_{d,j} = T_{d,in} \tag{30}$$

$$S_{f,0} = S_{f,in} \tag{31}$$

$$S_{f,j} = S_{f,out} \tag{32}$$

$$S_{p,0} = 0 \tag{33}$$

$$S_{p,j} = 0 \tag{34}$$

$$m_{p,0} = m_{p,in} + \sum_{n=1}^{j} J_{wa,n} A_{m,n} \tag{35}$$

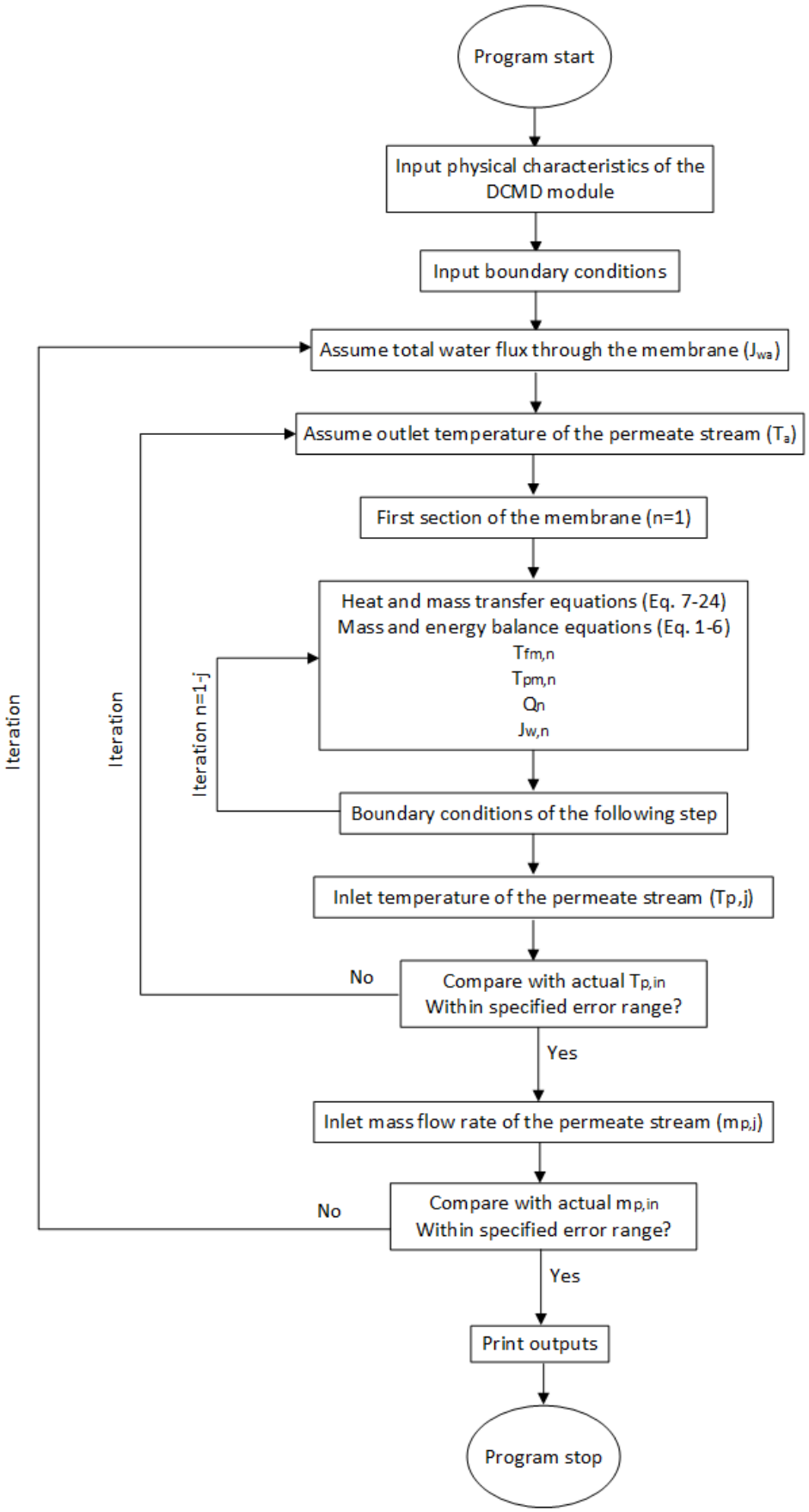

Fig. 3. Algorithm of the computation process for modelling the tubular DCMD

3. Experimental setup and instrumentation

3.1. Experimental setup description

Figure 4 depicts the components of the experimental setup. The system mainly consists of a tubular DCMD module; feed and permeate water storage tanks; a National Instrument Data Acquisition (NI-DAQ) unit; a power unit; two pumps; two flow meters; six thermocouples; a computer; valves; pipes; and fittings. The specifications of tubular DCMD are summarised in Table 1.

Sodium Chloride was dissolved in tap water to make the feed synthetic saline water and its salinity was constantly monitored using a conductivity meter. The saline water was heated up in the feed water storage tank using a 2 kW electric heater and its temperature was controlled by both a thermostat and a T-type thermocouple. Two pumps were used to circulate the feed and permeate flows in the hot and cold loops of the system. The flow rates of the feed and permeate streams were regulated via two valves located after the pumps and monitored using two flowmeters. Six thermocouples, which are monitored using a NI-DAQ system, were used to measure the temperatures at different points of the system. In order to record the data, LabVIEW 2014 software was used to write an application-based program interface and data was recorded at 10-second intervals.

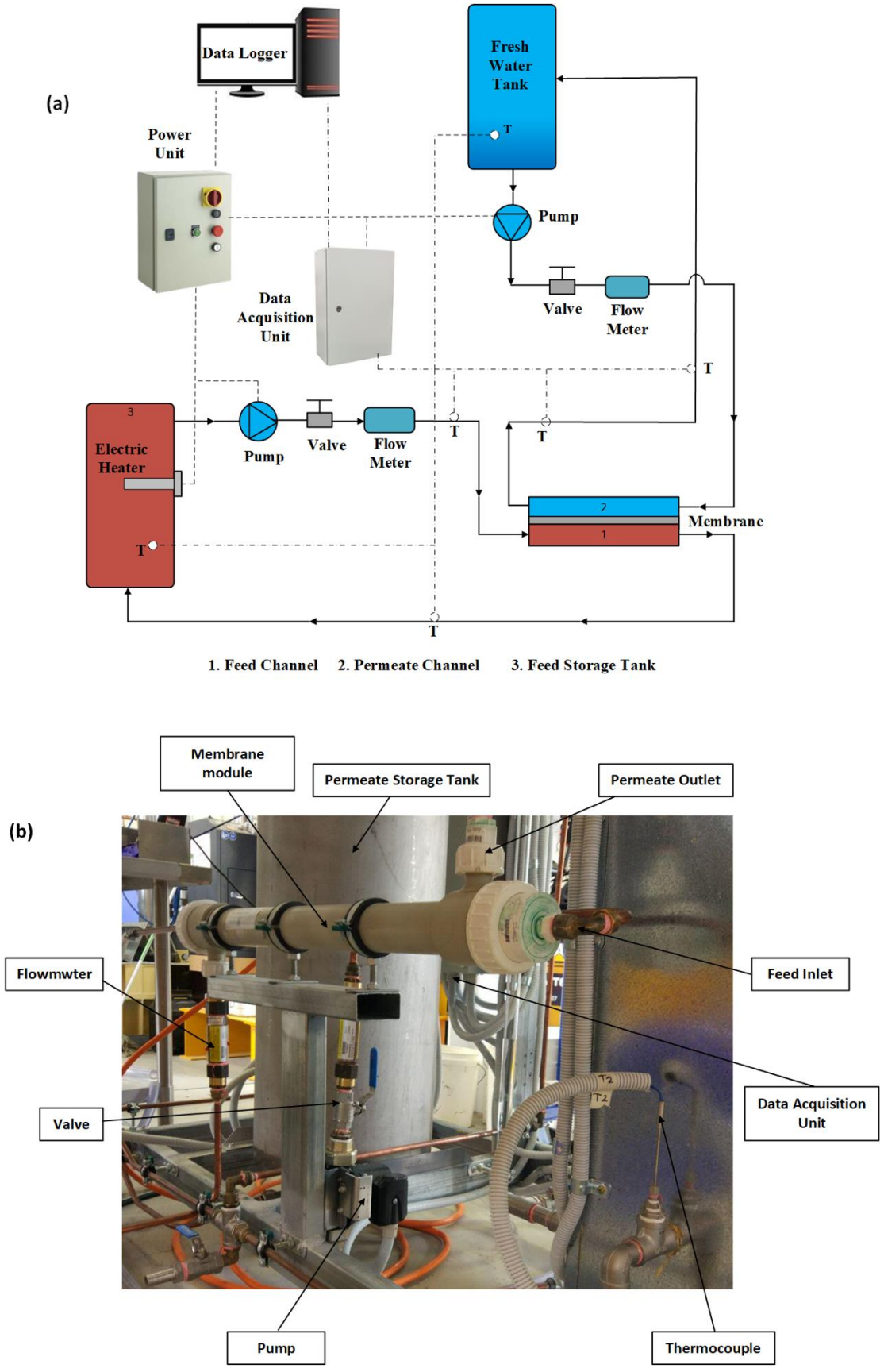

Fig 4. Components of the tubular DCMD setup: (a) schematic diagram, and (b) real picture.

Table 1. The specifications of the tubular DCMD module used in this study.

Characteristic	Value	Characteristic	Value
Model type	MD 090 TP 2N ANSI	Membrane material	Polypropylene
Nominal module diameter	9 cm	Membrane thickness	1.5 mm
Inner diameter of membrane module	5.5 mm	Outer diameter of membrane module	8.5 mm
Membrane module length	75 cm	Membrane porosity	75%
Membrane area	0.2 m^2	Potting material	Polypropylene
Average pore size	0.2 µm	Outer shell material	Polypropylene

3.2. Uncertainty analysis

The uncertainty of measured parameters includes systematic errors (i.e. calibration, data acquisition, and instrument accuracy) and random errors. The total uncertainty was estimated by applying the standard deviation method and was defined as [53]:

$$W_t = \sqrt{{\varepsilon_s}^2 + {\varepsilon_r}^2} \quad (36)$$

where, W_t represents the total uncertainty and ε_r and ε_s are the random and systematic errors, respectively, that can be calculated by [54]:

$$\varepsilon_s = \sqrt{\sum_{i=1}^{n} \varepsilon_{s,i}^2} \quad (37)$$

$$\varepsilon_r = \sqrt{\sum_{i=1}^{n} \varepsilon_{r,i}^2} \tag{38}$$

The parameter *n* in Eq. (37) and (38) represents the error source number and $\varepsilon_{r,i}$ can be obtained from [55]:

$$\varepsilon_{r,i} = \sqrt{\frac{\sum_{i=1}^{n}(\varphi_i - \bar{\varphi})^2}{N(N-1)}} \tag{39}$$

where $\bar{\varphi}$ and *N* represent the average value and the number of times a parameter is measured, respectively.

The propagation of errors method was applied to evaluate the uncertainty of the calculated parameters. The results uncertainty (W_R) can be determined by [56, 57]:

$$W_R = \sqrt{\sum_{i=1}^{n} \left(\frac{\partial R}{\partial x_i} W_i\right)^2} \tag{40}$$

where $R=R\,(x_1, x_2, \ldots, x_n)$

In Eq. (40), parameter *x* is an independent variable and *W* represents the uncertainty in that variable. Table 2 provides information about different calculated and measured quantities and their related uncertainties.

Table 2. Uncertainty analysis for measured and calculated quantities.

Parameter	**Measurement instrument**	**Operating range**	**Systematic uncertainty (± %)**	**Random uncertainty (± %)**	**Total Uncertainty (± %)**
Temperature	T-Type Thermocouple	-150 – 300 °C	1.42	0.32	± 1.7

Salinity	Conductivity meter	0-200 g/L	2.15	0.65	± 2.24
Flow rate	Flow meter	0 – 0.07 kg/s	1.34	0.45	± 2
TPC	-	-	-	-	± 4.3
GOR	-	-	-	-	± 5.6

4. Results and discussions

Figure 5 shows the variations of mass flux through the membrane wall based on different feed and permeate mass flow rates at different feed concentrations. The graphs clearly show that increasing mass flow rates positively affect the fresh water productivity. This is mainly because higher mass flow rates result in higher velocities and turbulence levels. The direct effect is the increase in the mixing which occurs inside the boundary layers resulting in higher heat and mass transfer coefficients. This effect can also be seen in Fig. 6 which shows the influence of feed and permeate mass flow rates on the heat transfer coefficient of both hot and cold streams. Increasing the mass flow rates from 5 to 20 L/min increases the hot and cold channel heat transfer coefficients by 3.19 and 4.27 kW/m^2K, respectively, resulting in water productivity increase of 15 g/m^2min at 35 g/L NaCl concentration. It is worth mentioning that Fig.6 was drawn by calculating the experimental heat transfer rate on both sides of the membrane considering the mass flow rates, specific heat capacities and inlet and outlet temperatures of the membrane module. Then, Eq. (8) and (10) were used to calculate the heat transfer coefficient on both feed and permeate sides of the membrane.

In addition, higher mass flow rate results in higher shear force which is generated between the fluid and the membrane surfaces which reduces the boundary layer thickness. This significantly decreases the effect of temperature and concentration polarization leading to lower temperature

difference between the membrane wall and bulk stream. This positively affects the mass flux because as the temperatures at the membrane interface get closer to bulk stream temperatures, the vapour pressure difference across the membrane which acts as the main driving force for vapour molecules increases leading to higher fresh water productivity.

Another interesting behaviour which can be seen in Fig. 5 is the steep slope of the graphs in the approximate mass flow rate range of 5 to 12 L/min which is mainly attributed to the change of state of flow from laminar to turbulent in this region named transition area. As the Reynolds number increases towards the turbulent region, the momentum and energy exchange enhances leading to higher heat transfer coefficient and mass flux through the membrane. Therefore, in large-scale applications, it is highly recommended to keep both the feed and permeate flow rate either near the end or beyond the transition range.

It can also be observed that for mass flow rate of 10 L/min for example, increasing the feed salinity slightly decreases the permeate water production mainly when salinity increases from 0 g/L to 10 g/L. Further increasing the feed stream salinity from 10 g/L to 20 and 35 g/L decreases the mass flux through the membrane by only 1.4 and 1.2%, respectively. Therefore, when the DCMD module is considered as a whole, the effect of salinity on the overall water production rate is considered insignificant comparing to the effect of other parameters such as feed temperature. This is primarily because increasing the salinity enhances concentration polarization leading to higher vapour permeation resistance across the membrane. Moreover, changing the feed water salinity changes the thermo-physical properties of the feed stream. For example, higher salinity of feed water reduces the thermal conductivity of the feed stream retarding the overall heat transfer process. However, the effect of increased salinity on thermo-physical properties is not as significant as the effect of variation of other parameters such as temperature. Therefore, the permeate productivity reduction due to increased salinity is not significant. In addition, higher salinity of feed stream increases the possibility of scaling and

fouling by covering some of the membrane's effective area which reduces the evaporation on the feed side and decreases the vapour pressure difference across the membrane. The key finding is that the permeate water productivity of the tubular DCMD module is independent of the feed water salinity.

Moreover, a good agreement can be seen between the theoretical and experimental results attesting the reliability of the developed multi-step theoretical model to predict the performance of tubular DCMD modules under different conditions. The major difference between theoretical and experimental data occurs in the transient area due to the fact that flow exhibits unpredictable behaviours in this region. The highest difference in this region occurs for salinity of 35 g/L and mass flow rate of 7.5 L/min where the predicted mass flux is 2.3 g/m^2min higher than the experimental data. These differences at mass flow rate of 7.5 L/min are 2, 1.93, and 1.9 g/m^2min for salinities of 0, 10, and 20 g/L, respectively.

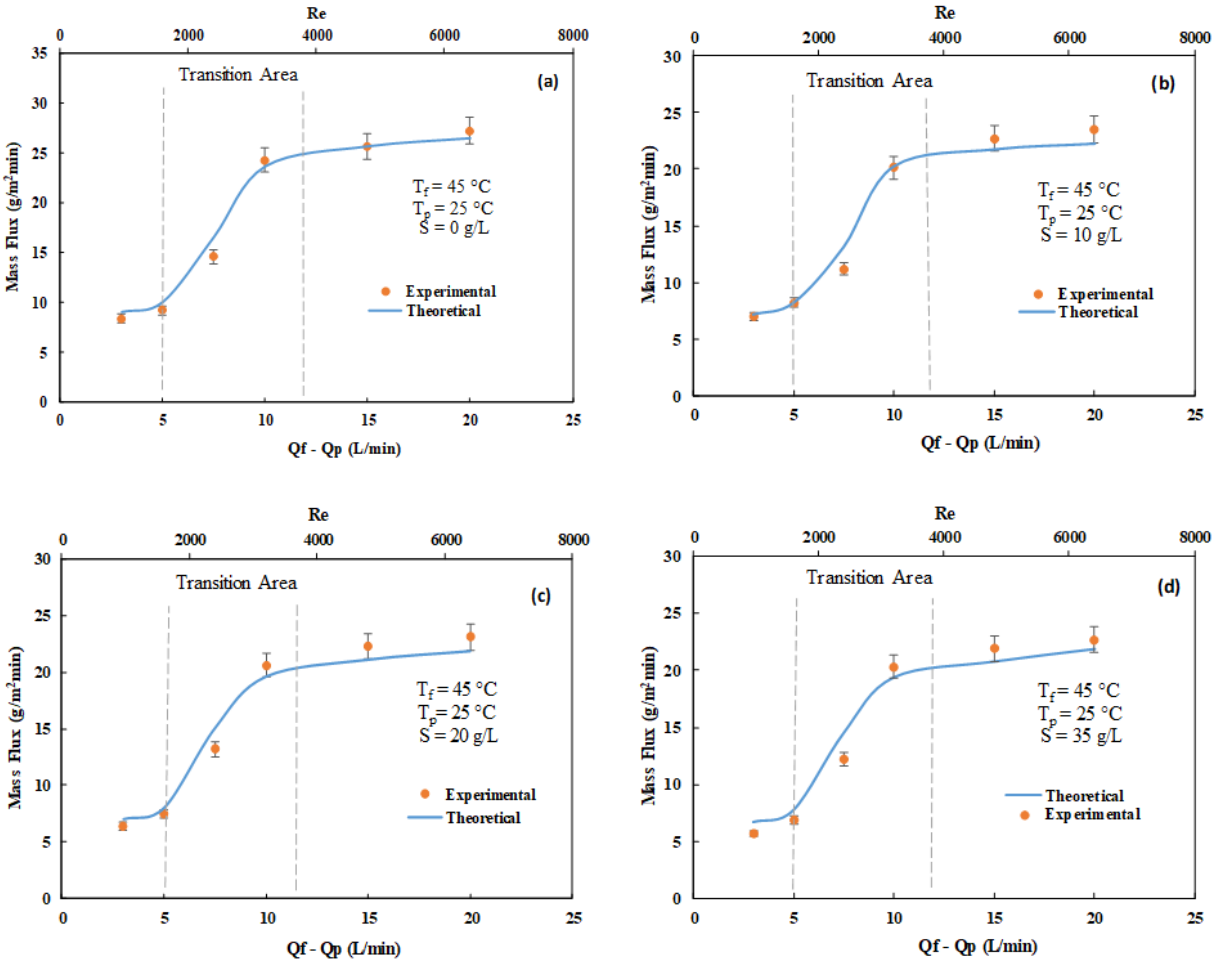

Fig. 5. Fresh water productivity based on different feed and permeate mass flow rates at different feed concentrations: (a) distilled water, (b) 10 g/L, (c) 20 g/L, and (d) 35 g/L (seawater)

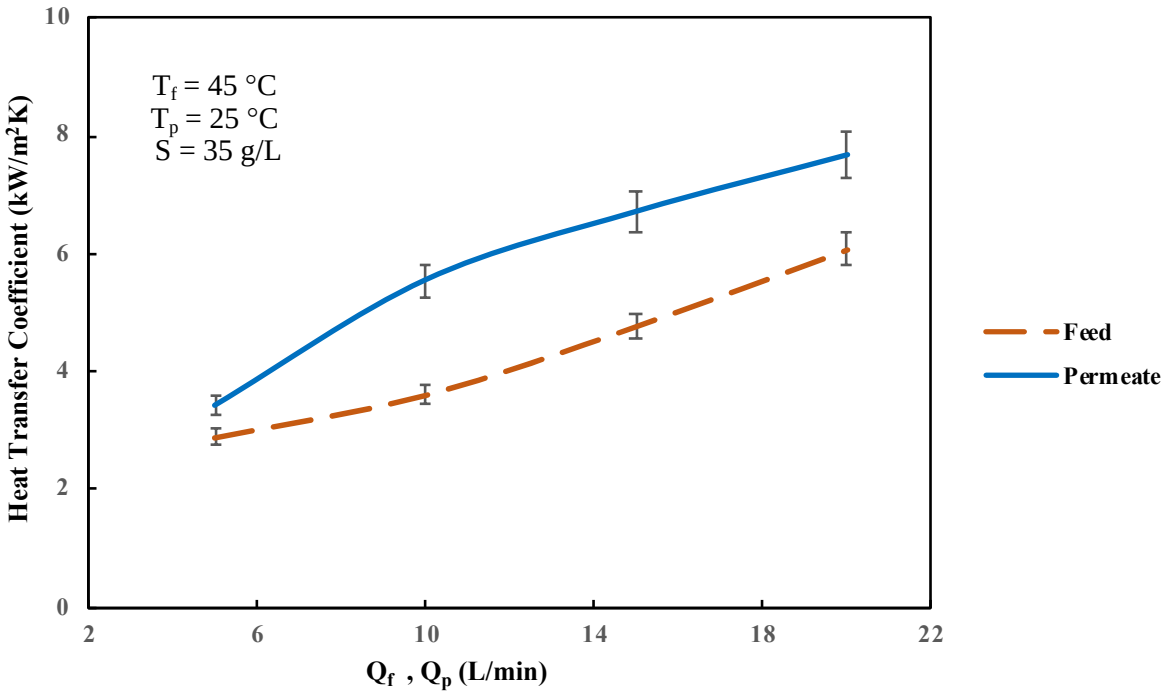

Fig. 6. The effect of feed and permeate mass flow rates on the heat transfer coefficient of hot and cold streams.

Figure 7 indicates the effects of feed and permeate temperatures on the fresh water productivity as a function of salinity. The mass flow rates of both channels were set at 10 L/min in the developed model while the permeate temperature in Fig. 8a was 25 °C and the feed temperature in Fig. 8b was 60 °C. At all salinities, higher feed temperatures as well as lower permeate temperatures result in higher water productivity. This is because the temperature and vapour pressure are directly related. Increasing the feed temperature increases the vapour pressure on feed side while decreasing the permeate temperature decreases the permeate side vapour pressure. Any or both of these changes increases the vapour pressure difference across the membrane, which acts as the main driving force of vapour movement across the membrane wall.

In addition, the slope of changes in permeate mass flux through the membrane is steeper at high feed and permeate temperatures. The main reason for this is that the relation between

temperature and vapour pressure is exponential. This means that the changes in vapour pressure with variation of temperature are more significant at high temperatures compared with low temperatures resulting in steeper mass flux increase or decrease through the membrane at high feed and permeate temperatures, respectively. Moreover, the data in Fig. 7 supports the independency of the tubular DCMD system's performance from feed water salinity. Although increasing the salinity of the feed stream enhances the concentration polarization, increases the vapour permeation resistance across the membrane, negatively affects the thermo-physical properties of the feed stream, and finally reduces the water productivity of the membrane, the effect of salinity on mass flux is not as significant as the effect of other parameters such as temperature. For instance, decreasing salinity from 20 to 10 g/L (i.e. 100% decrease) results in 2.8 g/m^{2}min increase in water productivity, while increasing feed temperature from 30 to 60 °C increases this parameter by 52 g/m^{2}min.

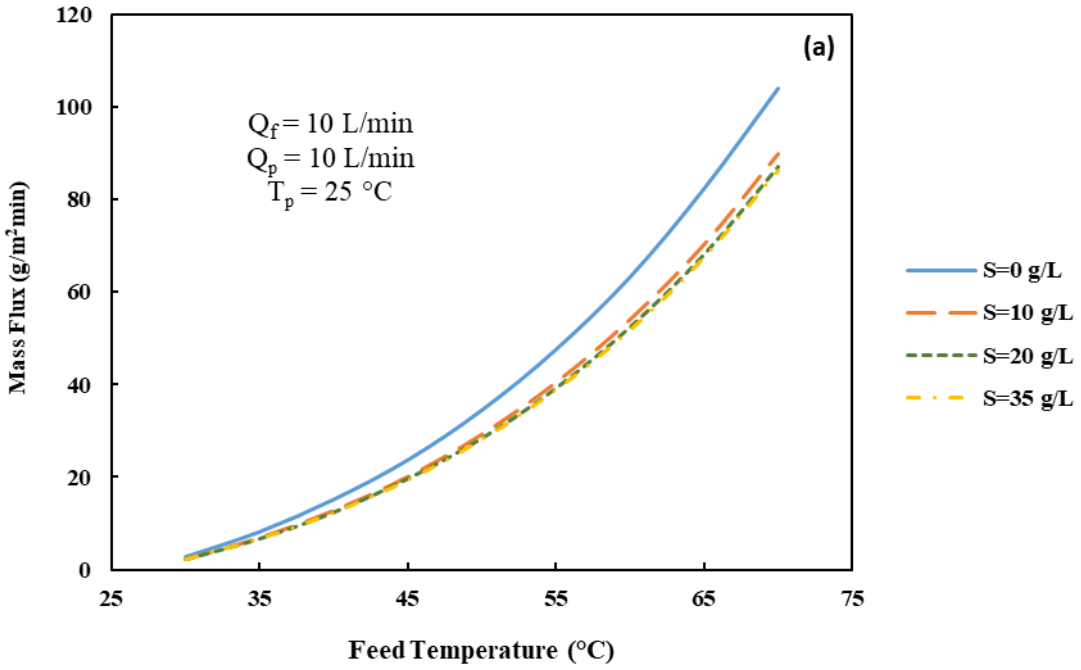

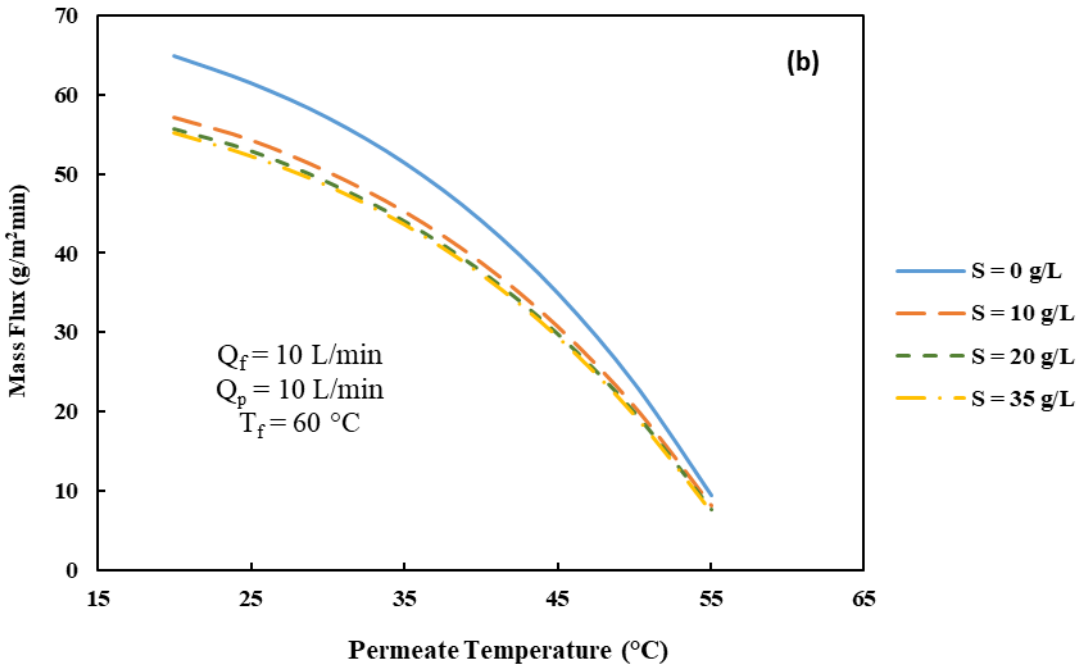

Fig. 7. Effects of (a) feed and (b) permeate temperature on water productivity of the tubular DCMD module as a function of feed salinity.

The water productivity increase percentage based on different feed and permeate temperatures is shown in Fig. 8. The bottom bars in Fig. 8 indicate the increase of water productivity at different permeate temperatures upon increasing the feed temperature from 50 °C to 60 °C. Similarly, the top bars depict the increase of water productivity at different feed temperatures upon decreasing the permeate temperature from 35 °C to 25 °C.

It can be seen that when feed temperature increases, the enhanced productivity is more significant at higher permeate temperatures. This suggests that percentagewise, running the DCMD system at higher feed temperature is more efficient in increasing the water productivity at high permeate temperatures. The increase percentage in water productivity by decreasing the permeate temperature has a declining trend at higher feed temperatures reaching the insignificant value of 5.5% at the feed temperature of 70 °C. Therefore, although running the DCMD system at lower permeate temperatures positively affects its fresh water productivity, this effect is significantly greater at lower feed temperatures.

Overall, while both increasing the feed inlet temperature and decreasing the permeate inlet temperature have a positive effect on the water productivity of the tubular DCMD systems, the former is noticeably more efficient than the latter.

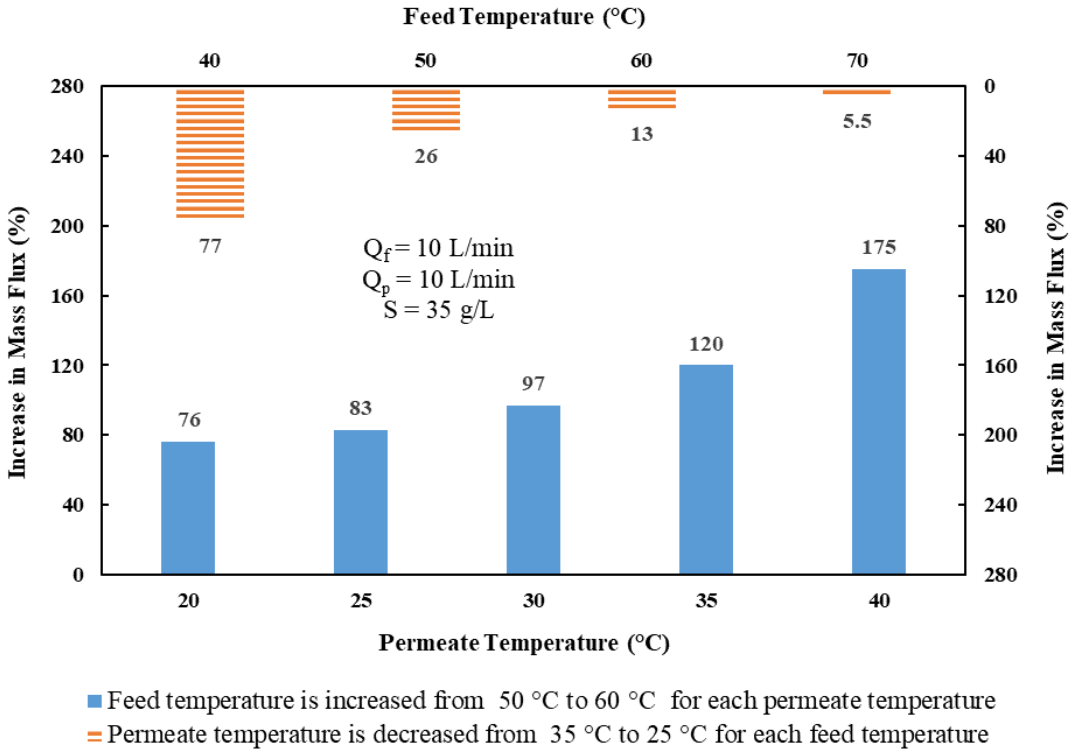

Fig. 8. Water productivity increase percentage of a tubular DCMD system based on different feed and permeate temperatures

Figure 9 depicts the changes in water productivity of the tubular DCMD system at various feed to permeate temperature ratios. The results show that the mass flux through the membrane increases exponentially albeit at different slopes depending on the permeate temperature. It can be seen that the variations slope decreases as the permeate water cools down from 40 °C to 20 °C. It is interesting to know that to reach the water productivity of 60 g/m^{2}min, for instance, the feed temperature should be set at 60 °C for permeate temperature of 20 °C, at 65 °C for permeate temperature of 30 °C, and at 69 °C for permeate temperature of 40 °C. This supports the results presented in Fig. 8 stating that to increase the water productivity of the tubular

DCMD system, heating up the feed stream is more effective than using the same amount of energy to cool the permeate stream down.

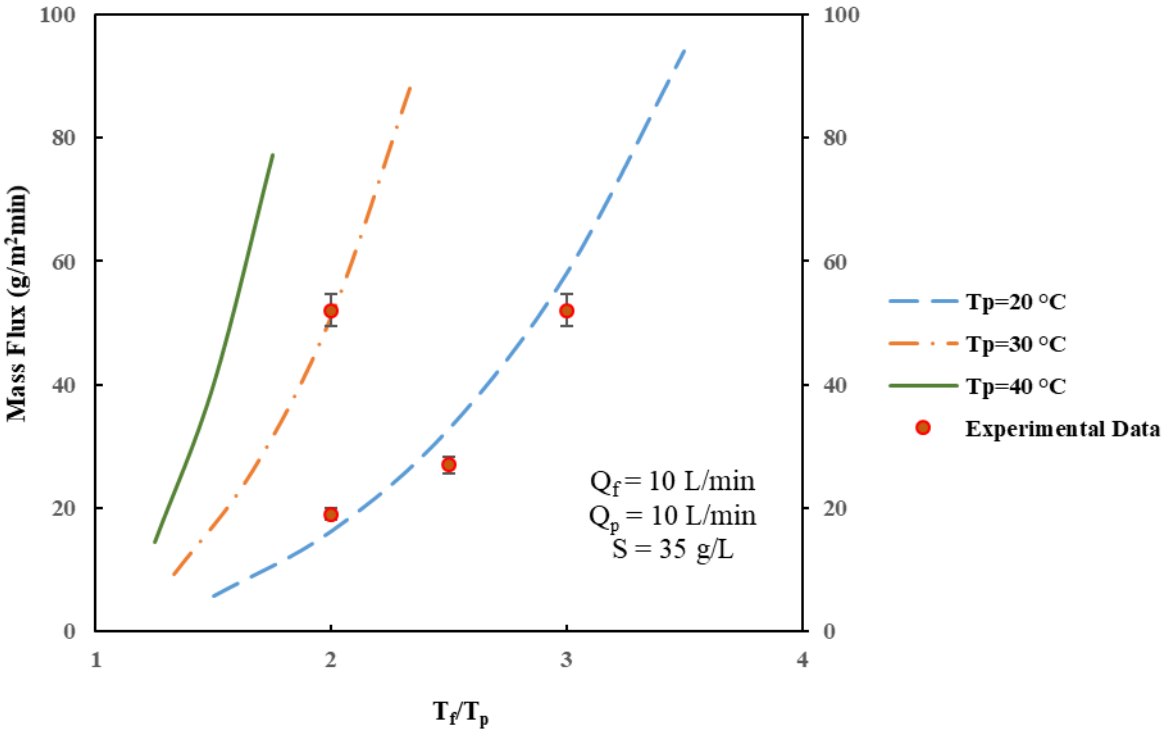

Fig. 9. Water productivity of the tubular DCMD system at various feed to permeate temperature ratios

For quantifying the influence of the temperature polarization on fresh water productivity of the tubular DCMD module, the temperature polarization coefficient can be calculated by [58]:

$$TPC = \frac{T_{f,m} - T_{p,m}}{T_f - T_p} \tag{41}$$

where, T_f (°C) and T_p (°C) are the average feed and permeate bulk temperatures at the inlet and outlet of the membrane module. Moreover, $T_{f,m}$ (°C) and $T_{p,m}$ (°C) are the average membrane surface temperatures at the hot and cold sides. As measuring the membrane surface temperature is almost impossible [9], the mean values obtained from the theoretical model were used for both theoretical and experimental calculations. The temperature polarization is one of the factors which retards the mass transfer driving force leading to lower water productivity.

Therefore, changing any parameter that increases the TPC and makes it closer to 1 is desirable. It should be noted that the purpose of considering changing trend and temperature polarization along the membrane module in the mathematical modelling of the DCMD module is not the removal of mean values from the studies, but to increase their accuracy.

Figure 10 indicates the changes of TPC as a function of the feed stream temperature at different feed mass flow rates. At all feed temperatures, increasing the feed mass flow rate has a positive effect on TPC. This is due to the fact that increasing the mass flow rate increases the Reynolds number and consequently the turbulence level, resulting in higher velocity and lower thermal boundary layer thickness. Consequently, the heat transfer rate increases and the temperature at the membrane wall gets closer to the respective bulk temperature.

Figure 10 also shows that at a constant feed mass flow rate, increasing the feed stream temperature leads to higher values of the TPC. Increasing the feed temperature changes the thermo-physical properties of the fluid such as thermal conductivity and dynamic viscosity. This results in higher heat transfer rate between the bulk stream and boundary layer and also higher turbulence level, and both of these parameters has a positive effect on the TPC. In addition, higher feed temperature increases the temperature difference across the membrane leading to higher convective heat transfer rate.

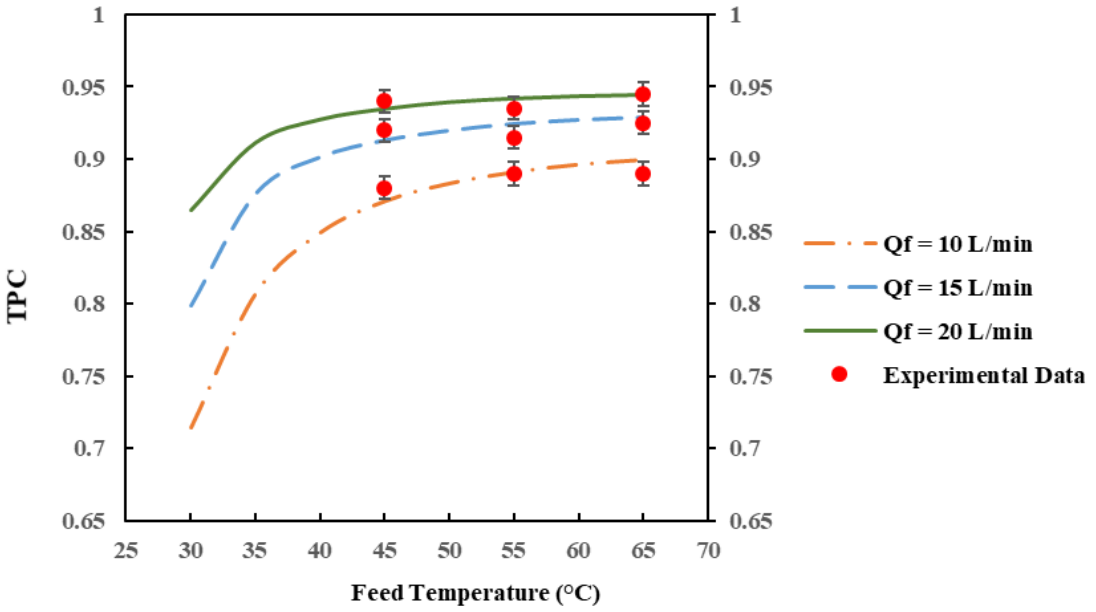

Fig. 10. Changes of temperature polarization coefficient (TPC) as a function of the feed stream temperature at different feed mass flow rates

Gained output ratio (GOR) is defined as the division of the vaporization latent heat of the produced distillate water by the thermal energy consumed in the feed channel [59]:

$$GOR = \frac{M_p H_v}{m_f C_{p,f}\left(T_{f,out} - T_{f,in}\right)} \tag{42}$$

Figure 11 shows the changes in GOR values based on feed temperature at various feed mass flow rates. The results indicate that at a constant feed temperature, increasing the feed mass flow rate has a positive effect on the GOR value. Higher mass flow rates lead to higher turbulence levels and lower boundary layer thicknesses which in return increases the heat transfer which occurs between bulk stream and boundary layer. This enhances the evaporation and hence, the GOR value increases. The results also demonstrate that increasing the feed temperature at a constant mass flow rate increases the GOR values. This is mainly due to the effect of temperature on the thermo-physical properties of the feed stream such as dynamic viscosity and thermal conductivity which consequently increases the heat transfer from bulk stream to boundary layer and enhances the evaporation.

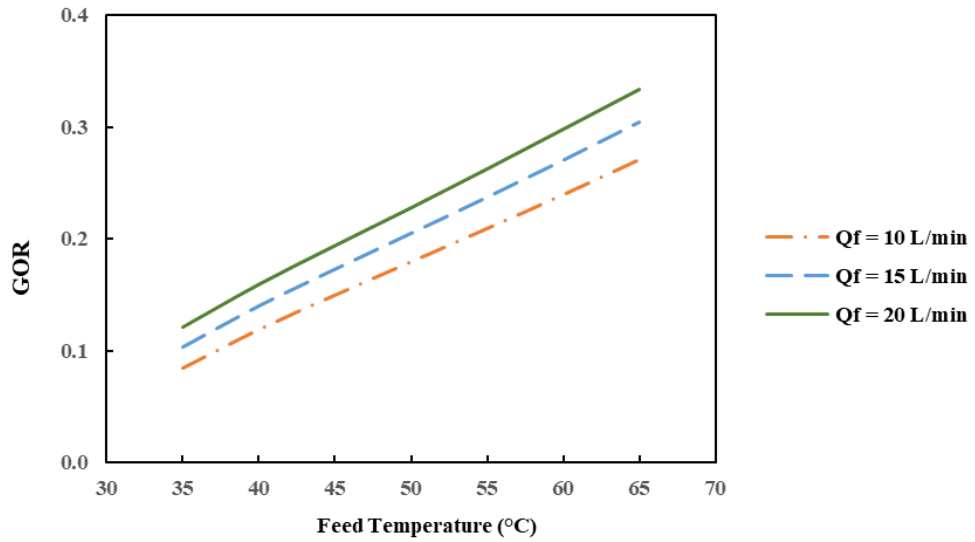

Fig. 11. Variations of GOR values based on feed temperature at various feed mass flow rates

Figure 12 indicates the effect of membrane's length on the water productivity of the tubular DCMD module at different feed temperatures. The results show that at all feed temperatures, the mass flux through the membrane decreases exponentially as the membrane's length increases. This is mainly due to the fact that as feed stream moves along the membrane, its salt concentration increases. Salinity increase not only enhances concentration polarization leading to higher vapour permeation resistance across the membrane, but also changes the thermo-physical properties of the feed stream. For example, higher salinity of feed water reduces the thermal conductivity of the feed stream affecting the overall heat transfer process negatively. Overall, higher salinity of feed stream retards the heat and mass transfer process leading to decrease in fresh water productivity.

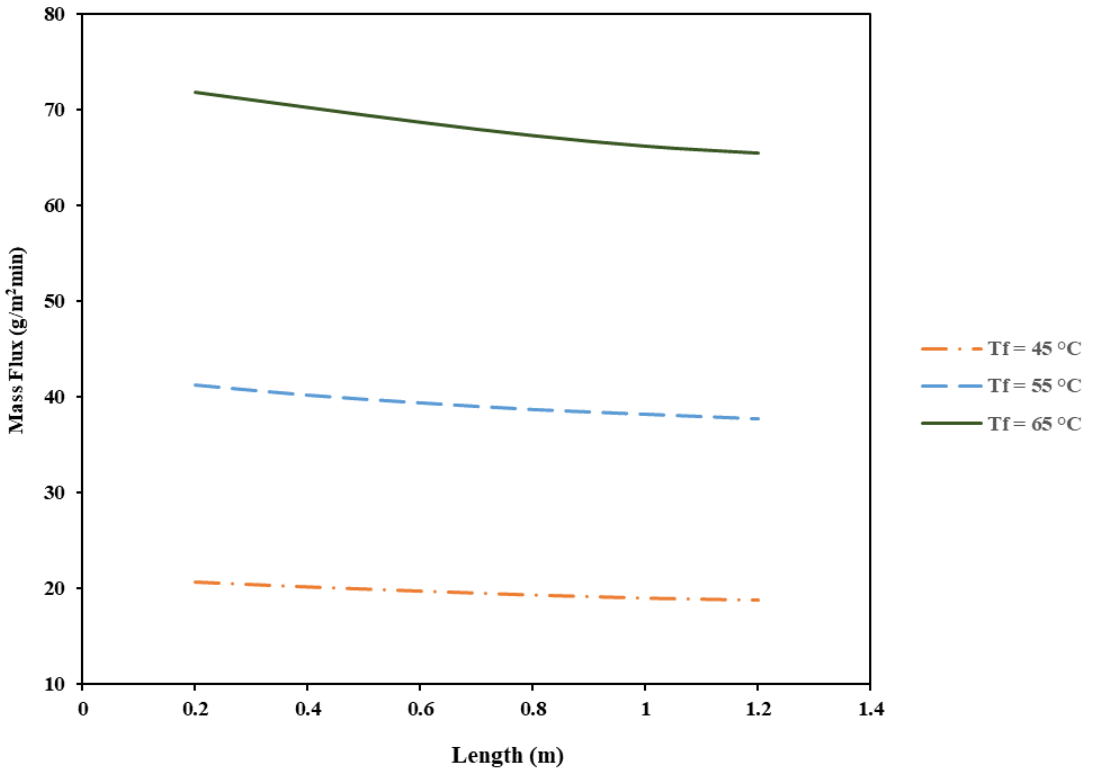

Fig. 12. Mass flux along the membrane at different feed temperatures

5. Conclusions

This study investigated the water productivity of a tubular DCMD system under different conditions both theoretically and experimentally. The results proved the capability of the developed model to accurately predict the performance of tubular DCMD modules even in large-scale applications in an economic manner. It was also found that the water productivity decreases noticeably upon increasing the membrane's length. The fresh water productivity of the tubular DCMD module is independent of the feed water salinity and increasing the mass flow rates have a positive effect on TPC and permeate water productivity of the tubular DCMD module. Based on the results, it is highly recommended to keep both the feed and permeate flow rate near or in the turbulent range of the flows. In addition, although increasing the mass flow rate increases the turbulence level, it decreases the residence time. Therefore, studying

the effect of residence time on water productivity of the tubular DCMD system can be the future research direction.

Acknowledgments

The authors would like to express their gratitude to Dr Alireza Mohyeddin for his kind assistance during the experimental phase of this project.

References:

[1] S.A. El-Agouz, Y.A.F.E.-. Samadony, A.E.Kabeel, Performance evaluation of a continuous flow inclined solar still desalination system, Energy Convers. Manage. 101 (2015) 606-615.
[2] N.A.S. Elminshawy, F.R. Siddiqui, G.I. Sultan, Development of a desalination system driven by solar energy and low grade waste heat, Energy Convers. Manage. 103 (2015) 28-35.
[3] V. Eveloy, P. Rodgers, L. Qiu, Hybrid gas turbine–organic Rankine cycle for seawater desalination by reverse osmosis in a hydrocarbon production facility, Energy Convers. Manage. 106 (2015) 1134-1148.
[4] W.F. He, D. Han, C. Yue, W.H. Pu, A parametric study of a humidification dehumidification (HDH) desalination system using low grade heat sources, Energy Convers. Manage. 105 (2015) 929-937.
[5] G. Zuo, R. Wang, R. Field, A.G. Fane, Energy efficiency evaluation and economic analyses of direct contact membrane distillation system using Aspen Plus, Desalination 283 (2011) 237-244.
[6] K. Nakoa, K. Rahaoui, A. Date, A. Akbarzadeh, Sustainable zero liquid discharge desalination (SZLDD), Sol. Energy 136 (2016) 337-347.
[7] A.M. Elzahaby, A.E. Kabeel, M.M. Bassuoni, A.R.A. Elbar, Direct contact membrane water distillation assisted with solar energy, Energy Convers. Manage. 110 (2016) 397-406.
[8] M. Khayet, Membranes and theoretical modeling of membrane distillation: a review, Adv. Colloid Interface Sci. 164 (2011) 56-88.
[9] M.R. Qtaishat, F. Banat, Desalination by solar powered membrane distillation systems, Desalination 308 (2013) 186-197.
[10] G. Rao, S.R. Hiibel, A. Achilli, A.E. Childress, Factors contributing to flux improvement in vacuum-enhanced direct contactmembrane distillation, Desalination 367 (2015) 197-205.
[11] D. Singh, K.K. Sirkar, Desalination of brine and produced water by direct contact membrane distillation at high temperatures and pressures, J. Membr. Sci. 389 (2012) 380-388.
[12] Y.M. Manawi, M.A.M.M. Khraisheh, A.K. Fard, F. Benyahia, S. Adham, A predictive model for the assessment of the temperature polarization effect in direct contact membrane distillation desalination of high salinity feed, Desalination 341 (2014) 38-49.
[13] S. Lin, N.Y. Yip, M. Elimelech, Direct contact membrane distillation with heat recovery: thermodynamic insights from module scale modeling, J. Membr. Sci. 453 (2014) 498-515.
[14] A. Gabelman, S.-T. Hwang, Hollow fiber membrane contactors, Journal of Membrane Science 159 (1999) 61-106.

[15] A.M. Karam, A.S. Alsaadi, N. Ghaffour, T.M. Laleg-Kiratia, Analysis of direct contact membrane distillation based on a lumped-parameter dynamic predictive model, Desalination 402 (2017) 50-61.
[16] T.-C. Chen, C.-D. Ho, H.-M. Yeh, Theoretical modeling and experimental analysis of direct contact membrane distillation, J. Membr. Sci. 330 (2009) 279-287.
[17] H. Guo, H.M. Ali, A. Hassanzadeh, Simulation study of flat-sheet air gap membrane distillation modules coupled with an evaporative crystallizer for zero liquid discharge water desalination, Appl. Therm. Eng. 108 (2016) 486-501.
[18] D.U. Lawal, A.E. Khalifa, Theoretical and Statistical Models for Predicting Flux in Direct Contact Membrane Distillation, Int. J. Eng. Research Applic. 4 (2014) 124-135.
[19] C.-D. Ho, H. Chang, T.-J. Yang, K.-Y. Wu, L. Chen, Theoretical and experimental studies of laminar flow hollow fiber direct contact membrane distillation modules, Desalination 378 (2016) 108-116.
[20] M. Berdasco, A. Coronas, M. Vallès, Study of the adiabatic absorption process in polymeric hollow fiber membranes for ammonia/water absorption refrigeration systems, Appl. Therm. Eng. 137 (2018) 594-607.
[21] F. Eleiwi, N. Ghaffour, A.S. Alsaadi, L. Francis, T.M. Laleg-Kirati, Dynamic modeling and experimental validation for direct contact membrane distillation (DCMD) process, Desalination 384 (2016) 1-11.
[22] M. Bhattacharya, S.K. Dutta, J. Sikder, M.K. Mandal, Computational and experimental study of chromium (VI) removal in direct contact membrane distillation, J. Membr. Sci. 450 (2014) 447-456.
[23] J. Zhou, X. Zhang, B. Sun, W. Su, Performance analysis of solar vacuum membrane distillation regeneration, Appl. Therm. Eng. 144 (2018) 571-582.
[24] H.C. Duong, P. Cooper, B. Nelemans, T.Y. Cath, L.D. Nghiem, Optimising thermal efficiency of direct contact membrane distillation by brine recycling for small-scale seawater desalination, Desalination 374 (2015) 1-9.
[25] A.E. Kabeel, M. Abdelgaied, E.M.S. El-Said, Study of a solar-driven membrane distillation system: Evaporative cooling effect on performance enhancement, Renew. Energy 106 (2017) 192-200.
[26] W.G. Shim, K. He, S. Gray, I.S. Moon, Solar energy assisted direct contact membrane distillation (DCMD) process for seawater desalination, Sep. Purif. Technol. 143 (2015) 94-104.
[27] D.J. Park, E. Norouzi, C. Park, Experimentally-validated computational simulation of direct contact membrane distillation performance, Int. J. Heat Mass Transfer 129 (2019) 1031-1042.
[28] M.R. Elmarghany, A.H. El-Shazly, M.S. Salem, M.N. Sabry, N. Nady, Thermal analysis evaluation of direct contact membrane distillation system, Case Studies in Thermal Engineering 13 (2019) 100377.
[29] N. Subramanian, A. Qamar, A. Alsaadi, A. Gallo Jr, M.G. Ridwan, J.-G. Lee, S. Pillai, S. Arunachalam, D. Anjum, F. Sharipov, Evaluating the potential of superhydrophobic nanoporous alumina membranes for direct contact membrane distillation, J. Colloid Interface Sci. 533 (2019) 723-732.
[30] N. Khumalo, L. Nthunya, S. Derese, M. Motsa, A. Verliefde, A. Kuvarega, B.B. Mamba, S. Mhlanga, D.S. Dlamini, Water recovery from hydrolysed human urine samples via direct contact membrane distillation using PVDF/PTFE membrane, Sep. Purif. Technol 211 (2019) 610-617.
[31] V. Perfilov, A. Ali, V. Fila, A general predictive model for direct contact membrane distillation, Desalination 445 (2018) 181-196.
[32] R. Ullah, M. Khraisheh, R.J. Esteves, J.T. McLeskey Jr, M. AlGhouti, M. Gad-el-Hak, H.V. Tafreshi, Energy efficiency of direct contact membrane distillation, Desalination 433 (2018) 56-67.
[33] W. Jantaporn, A. Ali, P. Aimar, Specific energy requirement of direct contact membrane distillation, Chemical Engineering Research and Design 128 (2017) 15-26.
[34] F. Li, J. Huang, Q. Xia, M. Lou, B. Yang, Q. Tian, Y. Liu, Direct contact membrane distillation for the treatment of industrial dyeing wastewater and characteristic pollutants, Sep. Purif. Technol. 195 (2018) 83-91.
[35] S. Ferrer, A. Mezquita, V. Aguilella, E. Monfort, Beyond the energy balance: Exergy analysis of an industrial roller kiln firing porcelain tiles, Appl. Therm. Eng. 150 (2019) 1002-1015.

[36] R.D. Gustafson, J.R. Murphy, A. Achilli, A stepwise model of direct contact membrane distillation for application to large-scale systems: Experimental results and model predictions, Desalination 378 (2016) 14-27.
[37] M.H. Sharqawy, J.H. Lienhard, S.M. Zubair, Thermophysical properties of seawater: a review of existing correlations and data, Desalin. Water Treat. 16 (2010) 354-380.
[38] A. Alkhudhiri, N. Darwish, N. Hilal, Membrane distillation: a comprehensive review, Desalination 287 (2012) 2-18.
[39] S. Srisurichan, R. Jiraratananon, A. Fane, Mass transfer mechanisms and transport resistances in direct contact membrane distillation process, J. Membr. Sci. 277 (2006) 186-194.
[40] M. Qtaishat, T. Matsuura, B. Kruczek, M. Khayet, Heat and mass transfer analysis in direct contact membrane distillation, Desalination 219 (2008) 272-292.
[41] F. Incropera, P. Frank, Fundamentals of Heat and Mass Transfer, New York: Wiley, 2002.
[42] M. Qtaishat, Design of Novel Membrane for desalination by membrane distillation, PhD Dissertation: University of Ottawa, 2008.
[43] G. Li, L. Zhang, Conjugate heat and mass transfer in a cross-flow hollow fiber membrane bundle used for seawater desalination considering air side turbulence, J Membr Sci 533 (2017) 321-335.
[44] R.K. Shah, D.P. Sekulić, Fundamentals of Heat Exchanger Design, John Wiley & Sons, Inc. , New jersey, 2007.
[45] H. Cheng, Y. Ju, Y. Fu, Thermal performance calculation with heat transfer correlations and numerical simulation analysis for typical LNG open rack vaporizer, Appl. Therm. Eng. 149 (2019) 1069-1079.
[46] Y. Yun, R. Ma, W. Zhang, A.G. Fane, J. Li, Direct contact membrane distillation mechanism for high concentration NaCl solutions, Desalination 188 (2006) 251-262.
[47] S.O. Olatunji, L.M. Camacho, Heat and Mass Transfer in Modeling Membrane Distillation Configurations: A Review, Frontiers in Energy Research 6 (2018) 130.
[48] T.K. Sherwood, R.L. Pigford, C.R. Wilke, Mass Transfer, McGraw-Hill, New York, 1975.
[49] U.L. Dahiru, E.K. Atia, Theoretical and statistical models for predicting flux in direct contact membrane distillation, J. Eng. Res. Applicat. 4 (2014) 124-135.
[50] K. Nakoa, K. Rahaoui, A. Date, A. Akbarzadeh, Sustainable zero liquid discharge desalination (SZLDD), Sol. Energy 135 (2016) 337-347.
[51] R.A. Johnson, M.H. Nguyen, Understanding Membrane Distillation and Osmotic Distillation, John Wiley & Sons, Inc., USA, 2017.
[52] M. Khayet, Membranes and theoretical modeling of membrane distillation: A review, Advances in Colloid and Interface Science 164 (2011) 56-88.
[53] R. Daghigh, A. Shafieian, Theoretical and experimental analysis of thermal performance of a solar water heating system with evacuated tube heat pipe collector, Applied Thermal Engineering 103 (2016) 1219-1227.
[54] A. Shafieian, M. Khiadani, A. Nosrati, Thermal performance of an evacuated tube heat pipe solar water heating system in cold season, Applied Thermal Engineering 149 (2019) 644-657.
[55] A. Shafieian, J.J. Osman, M. Khiadani, A. Nosrati, Enhancing heat pipe solar water heating systems performance using a novel variable mass flow rate technique and different solar working fluids, Solar Energy 186 (2019) 191-203.
[56] J.P. Holman, Experimental Methods for Engineers, 8th ed., McGraw-Hill, 2011.
[57] R. Daghigh, A. Shafieian, Energy-exergy analysis of a multipurpose evacuated tube heat pipe solar water heating-drying system, Experimental Thermal and Fluid Science 78 (2016) 266-277.
[58] F. Lagan, G. Barbiere, E. Drioli, Direct contact membrane distillation: modelling and concentration experiments, J. Membr. Sci. 166 (2000) 1-11.
[59] K. Jaochim, W. Marcel, R. Matthias, Solar thermaldriven desalination plants based on membrane distillation, Desalination 156 (2003) 295-304.